A Multi-Mode, Multi-Frequency Dielectric Elastomer Actuator

Sebastian Gratz-Kelly, Gianluca Rizzello, Marco Fontana, Stefan Seelecke, and Giacomo Moretti*

This paper presents a principle to develop multi-function dielectric elastomer actuators (DEAs) that can concurrently accomplish linear actuation and sound generation through a single electrical input. A centimeter-scale cone-shaped DEA is fabricated using silicone-based dielectric and electrodes. Measurements of the vibro-acoustic response reveal that the pumping deformation of the DEA contributes to a negligible extent in the sound generation, which is hence ascribable to higher order structural modes whose frequency pass-band is highly uncoupled from that of the pumping mode. Exciting the DEA with a multi-chromatic input voltage allows achieving strokes close to 1 mm or blocking forces over 0.5 N, while simultaneously generating sound pressure levels over 60 dB, regardless of possible forces and/or mechanical constraints on the DEA pumping motion. The ability of the DEA to concurrently generate linear actuation and sound is demonstrated via proof-of-concept tests: the DEA can reproduce music, while at the same time generating a deformation pulse or lifting a load comparable with its own blocking force. Furthermore, measuring the current generated by the DEA allows detecting deformations impressed by the exterior and use the DEA as an active audio-tactile interface, which produces a combined vibro-acoustic stimulus in response to a user's touch.

1. Introduction

Since their first appearance on the scientific stage, in the early 2000s,[1] dielectric elastomers (DEs) have established themselves as one of the most promising technologies to build centimeter/millimeter-scale electrostatic actuators, and have been indicated as a potentially game-changing solution in a broad variety of applications, ranging from mobile robots[2] to wearable assistive devices.[3]

DE actuators (DEAs) rely upon thin stretchable electrically-insulating polymeric membranes that can deform in response to a voltage difference applied on compliant electrodes covering their surface. These voltage-driven deformations are due to Coulomb forces between opposite charges on the DE's electrodes, which generate a compressive stress (the Maxwell stress) perpendicular to the electrodes, and cause the elastomer to squeeze in thickness and expand in surface.[4] DE materials available off-the-shelf, such as PDMS, acrylics or natural/synthetic rubber, can bear Maxwell stresses on the order of 0.1–2 MPa which, in turn, can induce strains over 100%.[1,5]

A point of strength of DEAs lies in the flexibility that they offer in terms of possible geometrical layouts[6–8] and combination with external force/stroke magnification mechanisms.[9–11] This led, in the past, to a flourishing of application demonstrators, including coin-sized pumps capable of output pressures of a few kilo-pascals and flows on the order of liters per minute;[12,13] soft grippers that can hold loads larger than their own weight;[14,15] and centimeter-scale walking robots capable of speeds over 1 body-length per second.[16] In addition to that, DEAs bear the ability to serve applications with frequency working ranges spanning several orders of magnitude ($10^{-1} – 10^4$ Hz[1]). Examples of high-frequency applications of DEs are haptic devices capable to provide feedback in the hundred-Hertz region,[3,17] or coil-free loudspeakers, which exploit the electrically-induced deformations of a DE diaphragm to generate sound waves.[18–20]

A relative unexplored ground, on which DEs might mark a real breakthrough, is that of multi-functionality. This is the combination of multiple independent functions, normally implemented via separate transducers, into a single unit, with the aim of pushing a system's bounds in terms of lightweight and compactness. Attempts to achieve multi-functionality via DEAs have mostly gone in the direction of self-sensing, which consists in determining a DEA's force/stroke based on measurement of its electrical state, with no need for external mechanical sensors.[21–23] This is typically achieved superposing a high-frequency small-amplitude component on top of the actuation driving voltage, and using the resulting measured current to infer information on the DEA state.[23,24]

S. Gratz-Kelly, G. Rizzello, S. Seelecke, G. Moretti
Intelligent Material Systems Laboratory
Department of Systems Engineering
Saarland University
Eschberger Weg 46, 66121 Saarbrücken, Germany
E-mail: giacomo.moretti@imsl.uni-saarland.de
M. Fontana
Institute of Mechanical Intelligence
Scuola Superiore Sant'Anna
Via L. Alamanni, 13b, 56010 Pisa, Italy

**ADVANCED
SCIENCE NEWS**

www.advancedsciencenews.com

**ADVANCED
FUNCTIONAL
MATERIALS**

www.afm-journal.de

In this work, we introduce a principle to develop multi-function DE devices that can concurrently accomplish audible sound generation and linear actuation. Specifically, we consider a known reference DEA topology, called cone DEA.[9,23] We use optical measurements of voltage-driven deformations to show that the frequency response of this DEA system features two clearly distinct and resolved working ranges: a lower-frequency (LF) range where the actuator features a pumping-like linear motion, associated to the displacement of a massive rigid moving frame attached the DE membrane; and a higher-frequency (HF) range where no motion of the suspended rigid frame occurs, but where higher-order structural modes of the DEA membrane are excited.[25,26] We then show, with acoustic measurements, that no sensible acoustic pressure is produced within the pass-band of the pumping mode, and sound generation is only achieved as a consequence of the HF structural modes' excitation.[27,28] We leverage on these different dynamic behaviors at different frequencies to concurrently produce a linear motion and generate sound. This is achieved by exciting the DEA with a single multi-chromatic voltage input including a LF high-amplitude component (responsible for linear actuation) and a HF low-amplitude component (responsible for sound generation) that can be programmed independently. With this setting, a centimeter-scale DEA can concurrently achieve a linear stroke 0.8 mm (16% the DEA height at rest) and sound generation with level over 60 dB at a distance of 0.35 m from the speaker. Dually, blocking the axial motion of the DEA, the membrane can generate voltage-driven blocking force variations in the order of 0.5 N, while still producing sound with a similar pressure level as in the free case.

To practically prove the ability of the DEA to concurrently serve multiple purposes (linear actuation and sound generation) in different operating conditions, we present three proof-of-concept tests. First, we show that the DEA can reproduce complex audio signals, with level of 60–70 dB, while at the same time producing an axial movement or lifting a load of 20 g (roughly, 200 times the DE membrane mass). Finally, we show that electric current measurements can be used to provide the DEA with the additional ability to recognize deformations impressed by external loads. In particular, the DEA can be used to sense the deformations impressed by a user, and provide a vibrotactile stimulus and a superposed sound feedback. Despite their simplicity, these case studies demonstrate that DEA multifunctionality might be used in the future to develop compact lightweight multi-modal interfaces capable of collocated audio-tactile feedback,[29–32] or buttons with programmable audio and tactile click feedback.[33]

The multi-frequency, multi-mode principle proposed here leverages and takes advantage of some general features of DEAs, such as surface-distributed actuation which allows exciting different deformation modes of the same membrane via a single input. Compared to other multi-functional membrane actuators based on polymeric transducers (e.g., ferroelectric and electrostrictive polymers[34]), DEs exhibit a relatively low elastic modulus (on the order of $10^{-1} - 10^{0}$ MPa, as opposed for example, to 10^{3} MPa of PVDF-based ferroelectric polymers), and can achieve larger stretches (>100%, as opposed to typical maximum values close to 10% for ferroelectric or conducting polymers[34]). This combination of features allows them to undergo large actuation

strains (here used to produce linear actuation) while simultaneously being subject to small-amplitude vibrations (leading to sound generation). The specific cone DEA layout considered here further allows obtaining a convenient frequency response (characterized by clearly distinct regions where the DE membrane either features a pumping motion or structural vibrations) for multi-mode operation. Although the cone DEA layout has been largely used in the past separately as a linear actuator in the low-frequency range[12,23] or a loudspeaker,[19,28] this is the first work that proves that the two operation modes can be exploited at the same time. In contrast to other DE loudspeakers, which in most cases rely on a pneumatically-biased bubble-like DEA membrane,[18,20,35] here the use of a large suspended mass (the moving rigid frame) allows creating a large frequency gap between the band where the DEA provides linear actuation, and the region where structural modes with high modal density are excited and generate sound. In contrast to traditional coil-based loudspeakers with rigid cone diaphragm, the LF pumping motion here does not contribute in generating audible sound in the bass range,[36] but produces a usable force/displacement output instead. These features allow producing independent linear actuation and sound generation at the same-time by concurrent excitation of different vibration regimes.

Several works, in the past, exploited the dynamic behavior of DEAs (e.g., resonant behaviors) to enhance the actuation performance.[37] Among others, Shresta et al.,[38] developed a transparent resonating-cavity sound absorber, whose absorption bandwidth can be tuned changing the voltage of a microperforated wall made of DE. Linnebach et al.,[13] used the mechanical resonance of a cone DEA to maximize the continuum flow delivered by a fluidic actuator driven by the DEA and a coupled of check valves. Cao et al.,[39] developed a wing mechanism capable of flapping strokes over 30° driven by a resonant double-cone DEA. At the same time, other works investigated the high-frequency continuum dynamics and modal response of DE membranes, and identified potential applications in the fields of morphing optics, conveyors, and vibration control.[25,40–42] However, the present work represents the first attempt to concurrently exploit different eigenmodes of a same DE membrane to produce multiple outputs, and it is the first work in which multiple actuation outputs are achieved via a single functional DE unit.

The rest of the paper is structured as follows. Section 2.1 describes the DEA multi-function principle in terms of layout (Section 2.1.1), characterization of the vibroacoustic response (Section 2.1.2), and multi-output performance (Section 2.1.3). Section 2.2 discusses the case study applications. Section 3 presents conclusions and possible future developments.

2. Results

2.1. Layout, Dynamic Response, and Multi-Mode Operation

2.1.1. Layout and Dynamic Response

The considered DEA topology is shown in **Figure 1**a. The actuator, known as cone DEA,[9,43] consists an initially-flat active polymeric membrane mounted, with a certain pre-stretch, on

a holding frame with diameter d_o. The central portion of the membrane (with diameter d_i) is attached to a rigid output disc (OD). The active membrane is made of a stack of DE layers and compliant electrodes with alternated polarity. Increasing the number of layers allows increasing the actuator's blocking force. In the mounting equilibrium configuration, the membrane is deformed off-plane, in a conical fashion, by means of a biasing spring that provides the OD with an axial force.

When a voltage difference v is statically applied on the electrodes, Coulomb forces between opposite-sign charges generate an electrostatic stress σ_M, called the Maxwell stress, which acts on the electrodes' plane (along the principal deformation directions) and is proportional to the squared electric field in the DE[44]

$$\sigma_M = -\varepsilon \left(\frac{v}{t} \right)^2 \qquad (1)$$

where ε is the DE permittivity, t the local thickness of the DE membrane, and the ratio v/t is equal to the electric field along the DE thickness. Maxwell stress adds up to the elastic stress, causing a relaxation of the DE and, hence, an expansion in the membrane surface (and a reduction in thickness, due to incompressibility), which results in an axial motion of the OD.

Similarly,[10,23] the pre-loading spring used here is a non-linear biasing spring (NBS), which consists of an initially-flat metal foil, pre-compressed in the radial direction and buckled off-plane (Figure 1a,b). The response of the NBS in the neighborhood of the equilibrium working position features a
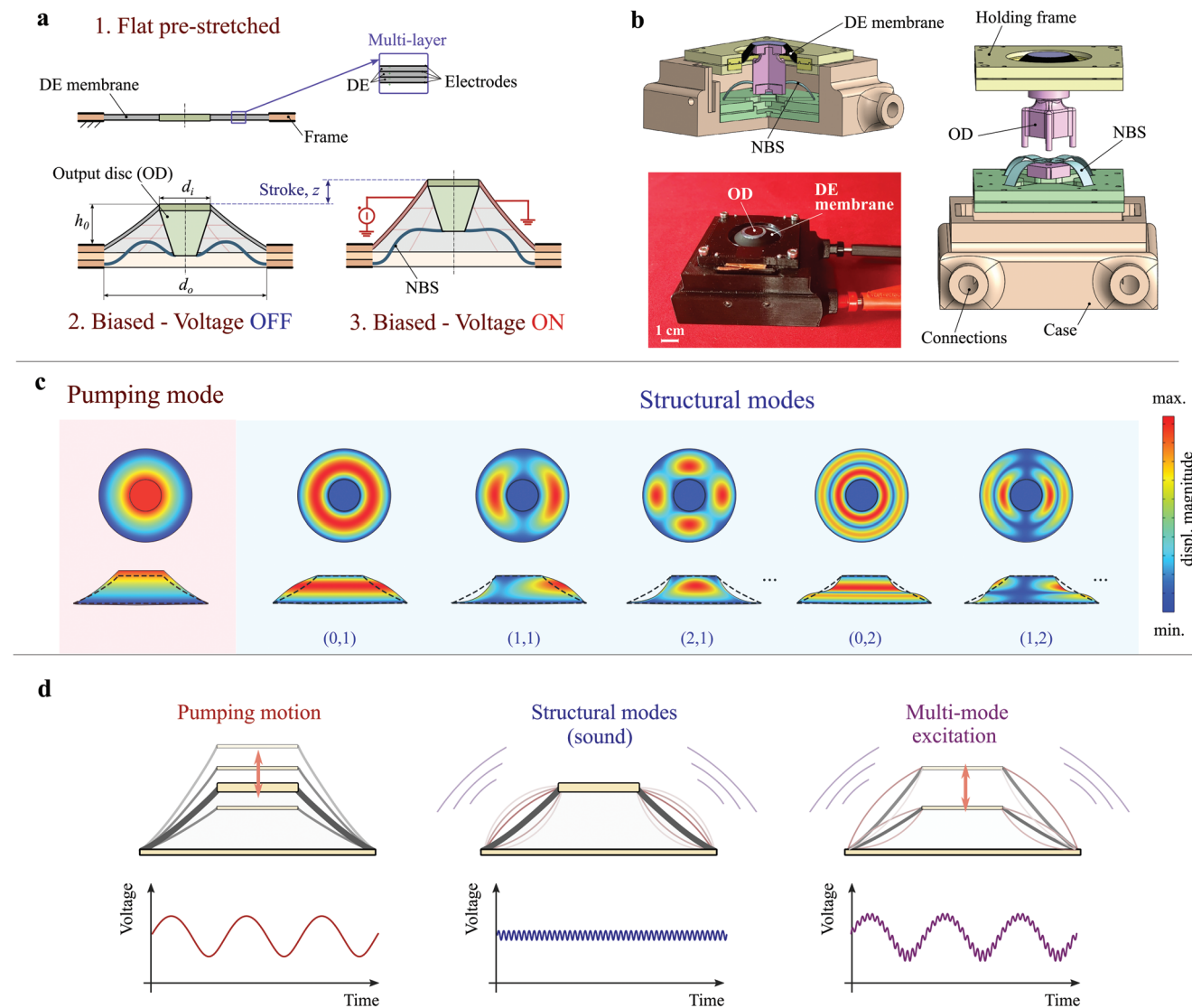

Figure 1. a) Cone-DEA layout: flat pre-stretched configuration (top left); mechanically-biased mounting configuration (bottom left); static deformation upon voltage application (bottom right). b) Prototype 3D model (assembled and exploded view) and photo. c) Deformation modes of the cone-DEA: low-frequency pumping mode (left) and high-frequency structural modes (right). Red areas in the contour plots indicate the regions where the oscillation amplitude is maximum, whereas blue areas indicate the regions where the displacement is minimum (nodes). The amplitude of the deformation in the structural modes is exaggerated for clarity of representation. d) Providing the DEA with an LF voltage input results in a linear motion, whereas applying a HF input excites one or more structural modes and results in sound generation. Superposing an LF and an HF input allows generating a linear stroke and sound at the same time.

negative-stiffness region, where an increase in the off-plane deformation causes a reduction in the NBS restoring elastic force (see Figure S3, Supporting Information). Such negative stiffness contribution partly balances out the axial stiffness due to the membrane elasticity, and allows achieving larger actuation strokes as compared to other positive-stiffness elastic biasing elements[10] (see Section S1, Supporting Information).

When subject to a time-varying voltage $v(t)$, the cone DEA response changes depending on the frequency content of the excitation voltage. At low-frequency, the DEA shows the same pistonic out-of-plane deformation pattern (i.e., axial displacement of the OD) as in the static case, hence behaving as a linear actuator. At high driving frequencies, the motion of the OD becomes negligible (low-pass filter behavior), that is, the DEA loses its ability to provide a linear stroke, but it can still generate sound as a result of the DE membrane's structural vibrations, that is, it behaves as a loudspeaker.

These different behaviors over different frequency ranges depend on the DEA's dynamics, which follow different deformation patterns (the deformation modes) based on the frequency of the electrical excitation. A set of deformation modes (including the low-frequency pumping mode and the higher-frequency structural modes) are qualitatively depicted in Figure 1c. In contrast to the low-frequency pumping mode, at high frequency the membrane exhibits a sequence of mode shapes, hereafter called structural modes, similar to those observed on flat annular tensioned membranes with fixed rims.[45] The OD motion is negligible for structural modes, since its mass is much larger than the membrane inertia.[26] We denote (m, n) a generic structural mode with m circumferential nodes and $n + 1$ radial nodes (including the central node and the fixed outer rim). Axial-symmetrical modes have no circumferential nodes, that is, they are of type $(0, n)$.

The ranges where the cone DEA exhibits either an out-of-plane "pumping" motion (linear actuation behavior) or structural vibrations (loudspeaker behavior) depend on the systems dimensions, the relative masses of the membrane and the rigid OD, the stresses (elastic+electrostatic) acting on the membrane, and the elasto-acoustic interactions (i.e., the air pressure load on the membrane caused by the membrane vibrations[20]). In our previous

work,[26] we presented and validated a model that allows estimating the frequency and modal response of cone DEAs, based on a constitutive electro-elastic description of the DE material.

Based on the frequency response of the DEA (Section 2.1.2), we hereby show that sound generation is ascribable to the structural modes, with negligible contribution from the pumping mode. Reciprocally, the axial motion of the OD filters out high-frequency voltage components present in the excitation. A broad gap exists between the frequency range where the DEA shows a pumping motion and the range where structural modes are excited. We take advantage of this feature to concurrently use the DEA as a linear actuator and a loudspeaker (Figure 1d), by separately exciting its deformation modes (the pumping mode and the structural modes) via multi-chromatic input voltage excitation (Section 2.1.3).

2.1.2. Vibro-Acoustic Response

We developed a prototype of cone DEA with an outer diameter $d_o = 30$ mm and inner diameter $d_i = 15$ mm, made of three 50-μm layers of silicone DE. We characterized the vibratory and acoustic response of the DEA subject to a time-varying voltage $v(t)$ in the following form

$$v(t) = \sqrt{U_0 + U_1 \tilde{v}(t)}, \text{ with } U_0 = V_b^2, U_1 = 2V_b V_a \tag{2}$$

where V_b is a constant bias voltage, V_a is a constant excitation amplitude, and $\tilde{v}(t)$ is a an excitation waveform with unit amplitude. The form of $v(t)$ in Equation (2) is chosen based on the analysis of the system linearized response. Because the DEA responds to the square of the applied voltage (see Equation (1)), a voltage in the form given by Equation (2) guarantees that the Maxwell stress variations are proportional to $\tilde{v}(t)$, in spite of the quadratic nonlinearity.[46] Notice that, if $V_a \ll V_b$, then $v(t) \simeq V_b + V_a \tilde{v}(t)$, that is, V_a roughly represents the amplitude of the time-varying component.

We concurrently measured the spectra of the average velocity on the DEA surface (DE membrane + OD)[26,42] and the acoustic response (**Figure 2**a), setting $\tilde{v}(t)$ equal to a periodic chirp.
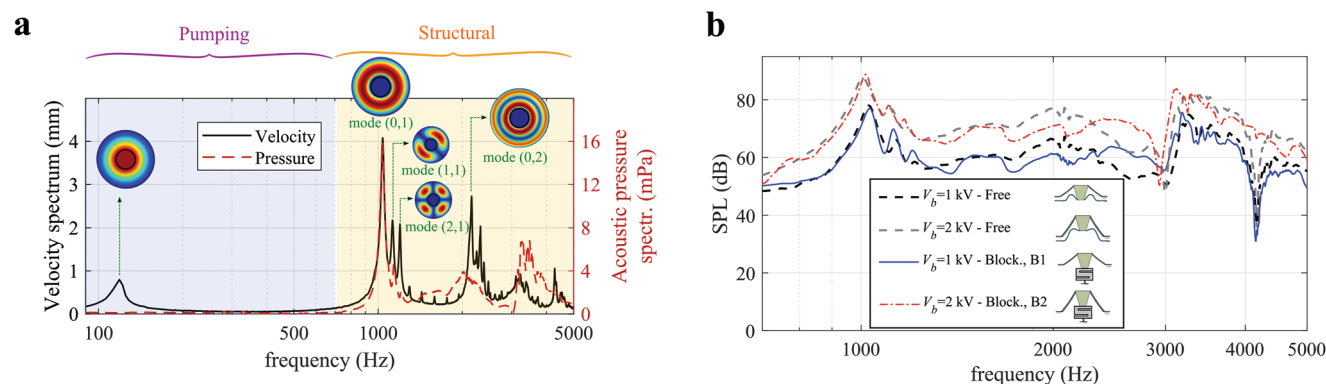
Figure 2. a) Spectra of the average axial velocity on the DEA surface and the resulting acoustic pressure (input voltage: chirp with $V_a = 100$ V and bias $V_b = 2$ kV). The DEA dynamics show two distinct regions: a pumping region (below 700–800 Hz) with a single isolated pumping mode, and a structural region characterized by high modal density. The DEA generates an audible sound within the structural region only. b) Sound pressure level at 0.35 m in front of the DEA (input: voltage sweep with amplitude $V_a = 100$ V and different bias levels). Two scenarios are considered: free OD (as in Figure 1a), and blocked OD. In each blocking test, the out-of-plane displacement of the DEA is set equal to the value measured at the same bias voltage in free conditions.

The velocity spectrum (solid line), measured with a laser Doppler vibrometer, presents a series of peaks corresponding to the different modes shapes of the DEA. The abscissa of the peaks roughly represents the natural frequencies of the associated modes. In the range below 600–700 Hz, the velocity spectrum has a single isolated peak in correspondence of the natural frequency of the pumping mode (119 Hz). At higher frequencies, the spectrum presents a set of peaks with high modal density, associated to the membrane structural modes (see Figure 1c). The first structural mode, namely (0,1), has a natural frequency of 1038 Hz. In the range under investigation (below 5000 Hz), the maximum average velocity is reached in correspondence of the axial symmetrical modes (pumping, (0, 1), (0, 2)). Although the DEA has an axial symmetrical shape, peaks corresponding to the non-symmetrical modes, for example, (1, 1), (2, 1), are also present. These are excited as a consequence of inhomogeneities in the layers thickness or higher order effects (e.g., aerodynamic loads or gradients in the voltage distribution due to the electrodes resistivity and the electrodes' connections to the circuit[47]).

Because of the large inertia of the OD (compared to the membrane mass), the natural frequency of the pumping mode is much lower than the natural frequencies of the structural modes, that is, the OD displacement practically falls to zero in the range where the structural modes are excited. The acoustic pressure spectrum (dashed line) shows that the DEA generates sound in the mid/upper-mid regions of the audible band. In particular, no acoustic output is generated in the range below 700 Hz, that is, sound is only generated as a result of the structural modes (with the pass-band of mode (0,1) representing the cut-in frequency for sound generation), with negligible contribution from the pumping motion.

This observation is confirmed by comparing the sound pressure level (SPL) generated by the DEA in free and blocking conditions, that is, with the OD free to move or locked in a fixed position respectively (Figure 2b). The SPL generated by the free DEA at a given bias voltage V_b is close to that measured in blocking conditions with the DEA subject to the same off-plane displacement as that measured in free conditions at that same bias voltage. Sensible differences (>2 dB) between the free and the constrained cases are only present over specific frequency ranges (e.g., 2300–3000 Hz) and they are ascribable to mounting misalignments in the blocking case, which affect the stress distribution over the DE.

The acoustic response is not uniform in the considered frequency range, as a result of the system's modal dynamics. The DEA generates a maximum SPL of 88 dB with bias voltage $V_b = 2$ kV, and 77 dB with $V_b = 1$ kV. This is achieved in correspondence of the natural frequency of structural mode (0,1). Compared to the other structural modes, mode (0,1) generates a sharper peak in the acoustic frequency response, because it features unidirectional (single-lobe) deformations of the DEA, which cause unidirectional alternated compression/expansion of the surrounding air. Increasing the bias voltage causes an increase in the SPL as a result of the reduction in stress generated by the electric field (Equation (1)), which causes the membrane vibration amplitude to increase. The decrease in stress due to the voltage also causes the peaks in the acoustic frequency response to shift toward left with increasing V_b. The

SPL responses shown in Figure 2b can be explained using multi-physics models that we developed in the past[28] (see Section S2.1, Supporting Information).

2.1.3. Multi-Frequency Multi-Mode Operation

We used the DEA prototype to concurrently produce a stroke (linear actuator working mode) and generate sound (loudspeaker working mode) by exciting it with a multichromatic input (Figure 1d), given by the sum of a bias, an LF term, and an HF term

$$v(t) = \sqrt{U_0 + U_1 \overline{v}(t) + U_2 \tilde{v}(t)}, \text{ with } U_0 = \frac{V_{max}^2 + V_{min}^2}{2},$$

$$U_1 = \frac{V_{max}^2 - V_{min}^2}{2}, \ U_2 = 2V_{max}V_a \tag{3}$$

where $\overline{v}(t)$ is an LF waveform with unit amplitude and fundamental frequency f_L; $\tilde{v}(t)$ is an HF waveform with unit amplitude and fundamental frequency f_H (with $f_H \gg f_L$); V_{max} and V_{min} are respectively the maximum and minimum values of the voltage due to the LF component (excluding the contribution of the small-amplitude HF component); and V_a is a parameter that roughly equals the amplitude of the HF component when the LF term has maximum value: notice indeed that, if $V_a \ll V_{max}$ and $\overline{v}(t) = 1$, then $v(t) \simeq V_{max} + V_a \tilde{v}(t)$. The LF component of the excitation (i.e., $U_1 \overline{v}(t)$) is responsible for the generation of a linear stoke of the OD. The HF component (i.e., $U_2 \tilde{v}(t)$) is responsible for sound generation.

The time-series of the OD stroke and the SPL are shown in **Figure 3**a,b for a case with $f_L = 3$ Hz (with $\overline{v}(t)$ equal to a sine and a trapezoid pulse respectively) and sinusoidal HF excitation with $f_H = 1108$ Hz (i.e., a $C_6^\#$). The DEA is able to concurrently generate a stroke on the order of 0.8 mm and a SPL on the order of 60–70 dB. Because the frequency range in which the DEA shows a pumping behavior does not present overlaps with the range where structural modes are excited (Figure 2a), the displacement z of the OD entirely filters out the HF component of the excitation. A slow drift in the OD position is only visible in the case of trapezoid LF excitation, but that is a result of the DE material viscosity. In contrast to that, an LF modulation (with the same frequency as the LF excitation) is present in the SPL. In particular, the sound intensity is higher when $\overline{v}(t)$ is maximum. This happen because the DEA stiffness associated to the structural modes varies with the applied voltage: increasing $\overline{v}(t)$ (and, hence, v) causes the stress on the DE membrane to decrease and leads to higher-amplitude structural vibrations (see also Figure 2b) and higher SPL. Technically, the LF variation in the DEA stiffness causes a beat in the DEA response, with a resulting acoustic output that holds spurious components (including, e.g., $f_H \pm f_L$) in addition to the fundamental (see Section S2, Supporting Information).

We observed that this distortion can be mitigated by introducing an LF compensation in the amplitude of the HF component in phase opposition with $\overline{v}(t)$. This was done by replacing V_a, in Equation (3), with a time-varying amplitude $v_a(t)$, which is maximum when $\overline{v}$ is minimum, and viceversa, namely

$$v_a(t) = [\alpha - (\alpha - 1)\overline{v}(t)]V_a \tag{4}$$

**ADVANCED
SCIENCE NEWS**

www.advancedsciencenews.com

**ADVANCED
FUNCTIONAL
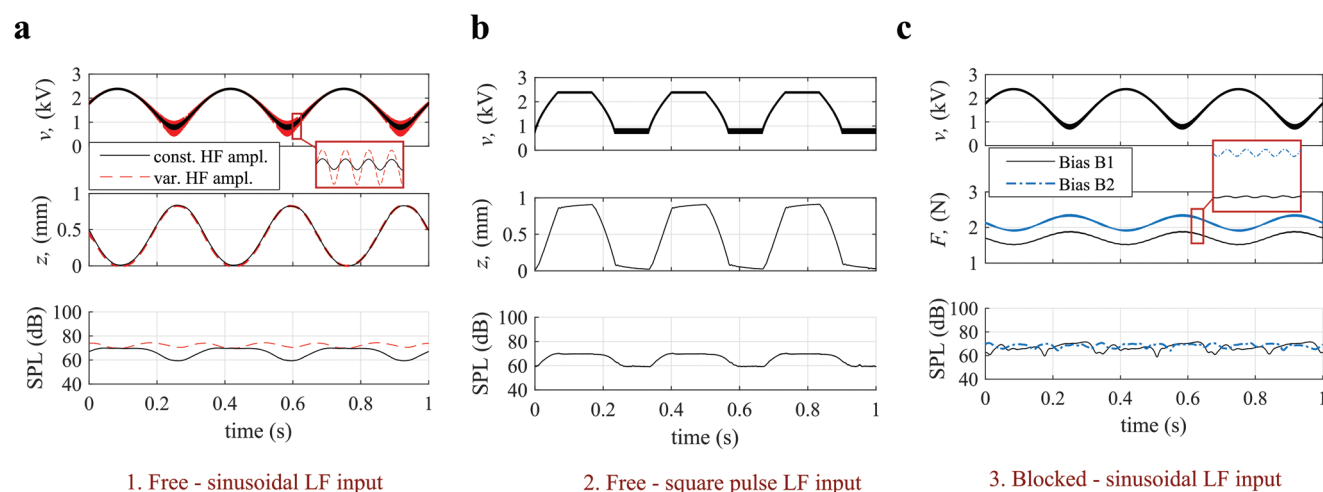MATERIALS**

www.afm-journal.de

Figure 3. Timeseries describing the DEA response to multi-chromatic voltage inputs: high-amplitude (V_{min} = 0.8 kV, V_{max} = 2.4 kV) low-frequency (f_L = 3 Hz) + low-amplitude (V_a = 0.1 kV) high-frequency (f_H = 1108 Hz, i.e., $C_6^\#$). a,b) Voltage, axial stroke, and SPL (moving-average) in free-displacement conditions with sinusoidal (a) and square (b) low-frequency input waveform. The black line refers to a constant-amplitude high-frequency pitch, whereas the red line refers to a variable-amplitude high-frequency pitch (Equation (4)). c) Voltage, axial force, and SPL in blocking conditions. The red and black lines refer to two different levels of mechanical biasing, corresponding to the positions assumed by the free DEA at V_{max} and V_{min}, respectively.

where α is a constant coefficient such that $\alpha \geqslant 1$. In the case of a 3 Hz LF sinusoidal excitation with a superposed 1108 Hz HF excitation (Figure 3a), using α = 2 (i.e., v_a varying in a range $V_a \leqslant v_a \leqslant 3V_a$) provides a more uniform trend in SPL (red dashed line) compared to the base case (black solid line), with maximum fluctuations on the order of 4 dB. The simple compensation strategy in Equation (4) and the corresponding results in Figure 3a here have the aim of highlighting margins and directions for equalizing the DEA sound output in the presence of a superposed linear actuation. Simple equalization strategies might be built using the heuristics in Equation (4), for example, by identifying a map of values of α that aims to obtain constant-level sound in the presence of different combinations of voltage bias, amplitude and HF excitation frequency. It is however worth remarking that the simple method proposed in Equation (4) does not keep into account the complexity of the system nonlinear response (i.e., the fact that the sound pressure is a complex function of the DEA state). For this reason, a more promising approach, and a direction for follow-up works, might be to build dynamic filters based on a model of the system. Compared to the simple logics in Equation (4), this might allow removing spurious harmonics from the sound output even in the presence of complex broadband multi-frequency excitations.

In blocking conditions (i.e., when the OD is locked), the DEA is able to produce sound with a level on the same order as that measured in free conditions at the same levels of voltage/deformation (Figure 3c). The SPL time trends differ from those in free conditions, as they are highly sensitive to misalignments and lateral loads in the blocking configuration. The reaction force generated by the blocked OD, which is proportional to v^2, contains both LF and HF components, with the latter showing a significantly smaller amplitude (on the order of 10 times) than the LF component, as a result of the small amplitude of the HF excitation. The maximum force variation (namely, the blocking force) produced by

the DEA between the maximum and minimum voltage is 0.5 N.

Figure 4 presents a summary of the multi-mode response of the DEA, subject to multi-frequency inputs, in terms of SPL (variation range) and force/stroke (variation over a period). For a given LF excitation (top row), changing the pitch f_H of the HF excitation ($C_6^\#$ to $C_8^\#$) does not cause significant modifications in the DEA free stroke or blocking force. Here the lowest considered pitch ($C_6^\#$) gives the largest SPL, as this frequency is the closest to the (0,1) spectral peak (see Figure 2). Varying the frequency f_L of the LF excitation for a given HF pitch (bottom row), the SPL and its variation range in time stay nearly constant. The blocking force is constant with the frequency, whereas the stroke is larger at the highest frequency (f_L = 30 Hz), which is closer to the natural frequency of the pumping mode (see Figure 2). The SPL is on the same order in free and blocking conditions, even though differences can be observed, especially in correspondence of the highest frequencies pitches ($C_8^\#$). As observed before, this is due to lateral misalignments introduced in the DE membrane in blocking conditions. This has a greater impact on the DEA acoustic response at higher frequencies, and are reflected by local differences in the sound spectra of in Figure 2b.

2.2. Proof-Of-Concept Tests

With the aim of providing a proof of the DEA's ability to combine linear actuation and sound generation, we hereby present three case studies, which demonstrate the actuator's multi-functionality in complex working scenarios. Each of the following case studies contributes in proving that the multi-mode principle introduced in Section 2.1 (where simple archetypal multi-frequency excitation inputs are considered) can be extended to advanced scenarios, where the DEA is subject to
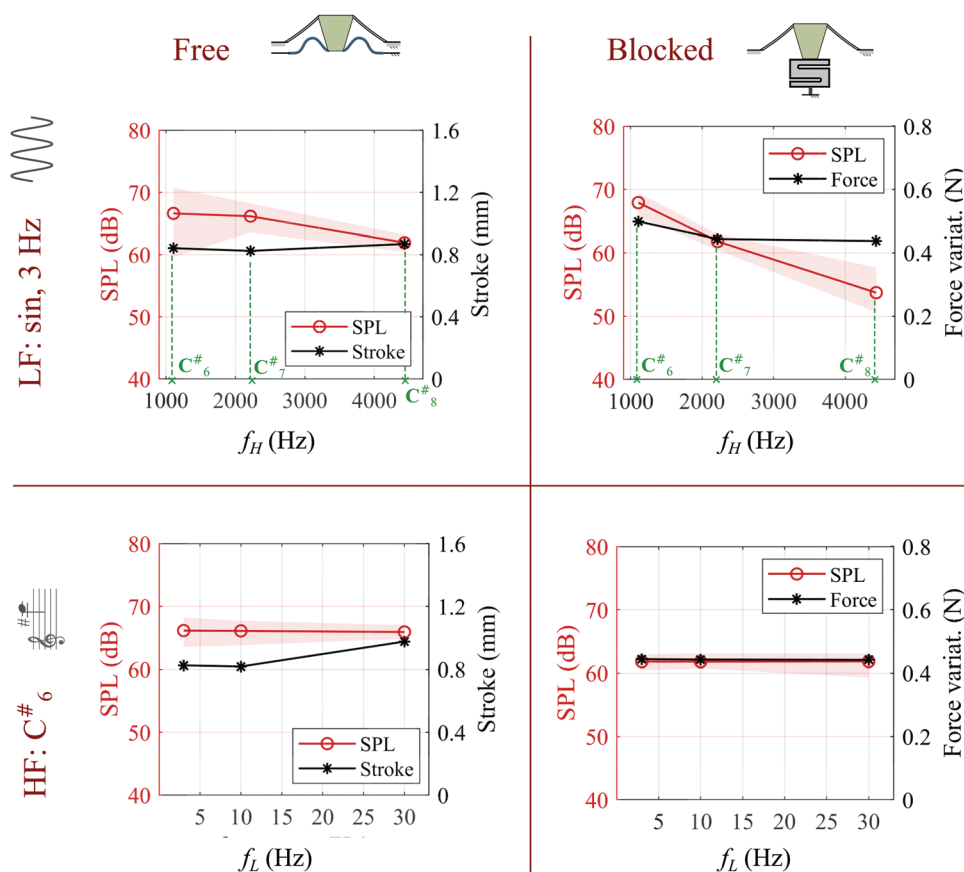
**ADVANCED
SCIENCE NEWS**
www.advancedsciencenews.com

**ADVANCED
FUNCTIONAL
MATERIALS**
www.afm-journal.de

Figure 4. SPL and stroke/force variation in the presence of multi-chromatic inputs, with V_{max} = 2.4 kV, V_{min} = 0.8 kV, and V_a = 0.1 kV. The left column refers to free-displacement tests, whereas the right column refers to blocking tests. The top row refers to constant LF sinusoidal excitation at 3 Hz, and different HF pitches; the bottom row refers to a constant HF signal of 1108 Hz ($C_6^\#$) and different LF sinusoidal excitations. The colored areas indicate the variation range of the SPL over time for the different tests.

complex excitation signals or complex boundary conditions. In particular,

- We first prove that linear actuation can be produced in combination with complex acoustic signals, by concurrently using the DEA as a speaker (that uses structural vibrations to play a tune) and a metronome (which produces a pumping motion in sync with the tune's beat).
- The same scenario as above (complex acoustic signals reproduction + linear actuation) can also be achieved when the DEA is subjected to a large external force (e.g., a weight applied on its end-effector, on the same order as the blocking force measured in Figure 4) that contrasts its linear actuation.
- Additionally to combined multi-frequency actuation, the DE membrane can incorporate a sensing function. For example, crossing voltage and current measurements allows the DEA to recognize a touch applied by a user on the OD and respond with a combined vibrotactile and acoustic stimulation.

For all presented proof-of-concepts, quantitative figures of merit are reported in the following and complemented with videos of the tests (see Supporting Information).

Whereas structured applications of the presented principle might be developed in the future, the simple tests reported

here show that a single DE active unit can concurrently accomplish complex linear actuation, sound generation, and sensing tasks. At the same time, the presented results provide indications for future application directions, including multi-modal collocated audio-tactile interfaces,[31] or virtual programmable buttons.[33]

Time-beating loudspeaker: The DEA can simultaneously work as a loudspeaker and a metronome, beating the tempo of the tune that it is reproducing through the axial movement of the OD (**Figure 5**a and Video S1, Supporting Information). This has been achieved by supplying the DEA with an input, v^2, which is the sum of a low amplitude HF component rendering the music track and a higher amplitude (V_{min} = 0.8 kV, V_{max} = 2.4 kV) LF square wave term with a fundamental frequency equal to the beat of the tune (here, 134 BPM). The amplitude of the HF component has been modulated over time as described in Equation (4), using V_a = 0.2 kV and α = 2.5. In the initial/final phases of the video, the DEA reproduces a clicking sound synchronized with the pumping movement (beat) of the OD. Following that, the DEA plays music while the upward movement of the OD concurrently marks the pulses of the measure. Plots in Figure 5a are relative to a portion of the experiment. The music line in the plot only shows the melodic line, whereas in the test the DEA played both melody and accompaniment.
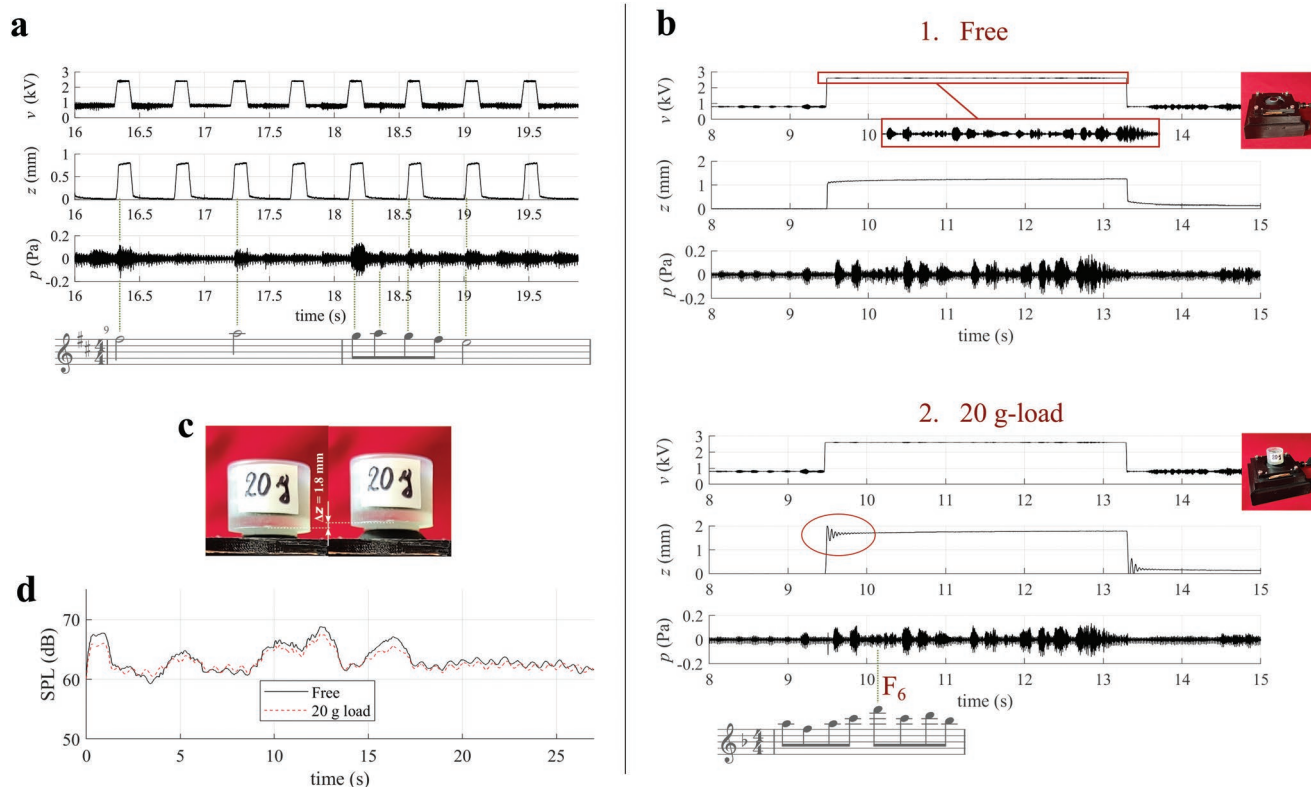
Figure 5. a) Time-beating loudspeaker. The plot shows an excerpt (two bars) of the timeseries of the applied voltage, the axial stroke, and the acoustic pressure. The DEA is driven with an input which is the sum of a high-frequency component responsible for the tune reproduction, and a low frequency component, causing the DEA OD to move upward in sync with the beats of the tune's tempo. b–d) DEA playing a tune under load. b) Excerpt of a time-series of voltage, stroke and acoustic pressure for the free DEA (top) and in the presence of a 20 g mass applied on the DEA's OD. c) Increasing the voltage from $V_{min} = 0.8$ kV to $V_{max} = 2.6$ kV causes the DEA to lift up the mass by 1.8 mm, while the tune is hitting the top notes. d) Time-trend of the SPL (moving-average) for the two cases with free and loaded DEA.

The stroke of the DEA OD on the beats is of 0.8 mm, whereas the average SPL during sound reproduction is 62 dB. Similar to the results discussed in Section 2.1.3, the OD movement is unaffected by the HF excitation. In contrast with pure tones, which are affected by a recognizable beat distortion caused by the superposed LF actuation (Figure 3), in this case the multichromatic nature of the reproduced tune masks such distortions to the listener's ear (see Video S1, Supporting Information).

Sound generation under load: Although in the previous case study the DEA is free from external applied loads (other than the forces due to the DE elasticity and the NBS), DEA is able to generate sound and linear actuation even under the effect of an applied load. We applied a mass of 20 g (i.e., comparable with the blocking force discussed in Figure 4) on the OD, and played music by applying an audio signal (song track) onto the DE (Video 2 and Figure 5b). The peak amplitude of the acoustic signal is on the order of 0.4 kV, and it is thus not sufficient to produce any axial motion of the OD, regardless of the waveform bandwidth. By applying a step variation (between $V_{min} = 0.8$ to $V_{max} = 2.6$ kV) on the bias voltage, the DEA can lift the mass while concurrently playing the music piece. Figure 5b compares the time-series of the OD displacement and the generated sound pressure for the two cases of free and loaded DEA (without and with loading mass respectively), in the presence

of a same input signal (piece-wise constant bias + soundtrack). The OD stroke is 1.2 mm in the free case and 1.8 mm in the loaded case (Figure 5c). In fact, when a mass is applied on the device, the initial value of the DEA's out-of-plane equilibrium displacement h_0 is lower, hence making a larger stroke available for the OD upon voltage application. The OD displacement is free from HF components due to the audio track, even though an underdamped oscillation is visible in the case with applied mass (oval inset). This is due to the free oscillation of the DEA+mass system, which has a natural frequency of 22 Hz (as opposed to 119 Hz of the free DEA). Figure 5d shows the trend of the SPL in the two cases with and without load. The SPL in the two cases is comparable, hence confirming that sound generation is loosely affected by constraints on the OD axial displacement. The SPL in the loaded case is, however, generally lower than that in free conditions. This is partly due to the fact that the out-of-plane deformation of the cone DEA is lower because of the applied mass, and partly due to shading effects due to the 20-g-mass body (aligned with the DEA axis).

Audio-tactile button: Measuring the output current allows inferring information on the DEA state and using it as a sensor, hence providing the system with a further functional layer, in addition to LF and acoustic actuation. If a bias voltage is applied on the DEA, a sudden change in the device configuration (and, hence, capacitance), for example, a touch,
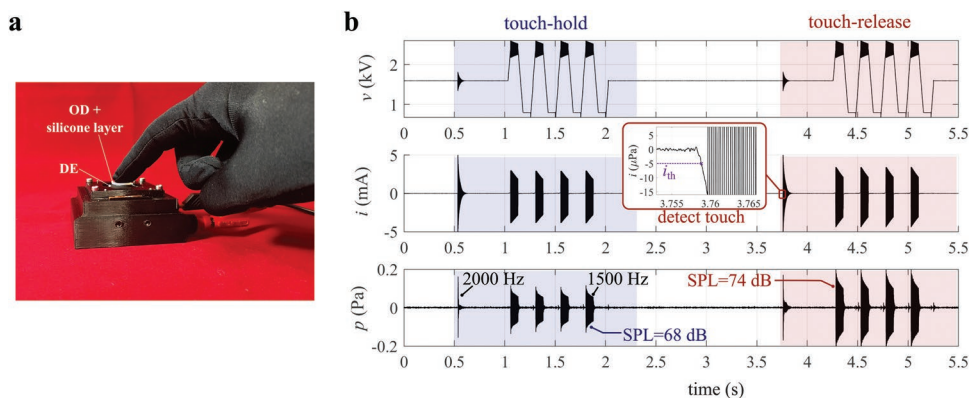
Figure 6. Audio-tactile DEA interface. a) Picture of a user pushing the DEA OD, hence triggering an audio-tactile response. b) A constant voltage of 1.6 kV is initially applied on the DEA. Pushing the interface with a finger causes a peak in the current. When the current surpasses a fixed threshold, the DEA responds with a complex feedback consisting of: a click sound (2 kHz frequency, with exponentially decreasing amplitude), followed by a low-frequency (4 Hz) axial motion of the OD and a superposed pulsated sound (1.5 kHz with exponentially decreasing amplitude). In the plots, the DEA repeats its routine twice: in the first iteration, the user pushes the DEA to trigger it and keeps it pressed all through the routine; in the second iteration, the user pushes the DEA and then removes the finger.

generates a current peak that can be used to trigger a response. We used the DEA as an audio-tactile button, able to sense a compression applied by a user on the OD and respond with an acoustic and a vibrotactile stimulus (**Figure 6** and Video S3, Supporting Information). Upon recognizing the user's touch via currents measurements, the button executes a pre-defined routine, consisting of: 1) a clicking sound, generated via a HF sinusoidal excitation with exponentially decreasing amplitude; and 2) a combined LF square wave excitation and a pulsated HF excitation (sine wave with exponentially decreasing amplitude), applied in correspondence of the phases in which the LF component is maximum. The latter produces a combined vibrotactile and acoustic feedback. Because the human vibrotactile range lies below 1000 Hz,[48] tactile stimulation here is entirely due to the LF component of the excitation, whereas the HF component only contributes a sound feedback. Note also that the DEA blocking force (see, e.g., Figure 4) is largely above (roughly, one order of magnitude) the finger's perceptual threshold,[49] that is, the DEA generates a clearly perceivable stimulus. Although, during operation, the users are constraining the axial pumping motion of the DEA OD through their finger, sound is still generated as a result of the DEA higher-order structural modes. Keeping a pressure applied on the OD upon touch results in SPLs of 68 dB (Figure 6b left), whereas releasing the OD after the touch results in a level of 74 dB (Figure 6b left). The difference between the two cases is due to the difference in the DEA bias axial deformation (the DEA is pushed downward when a touch is applied) and acoustic shielding due the user's hand (which partly covers the sound pattern toward the microphone).

Compared to conventional combined audio-tactile interfaces, which make use of separate transducers and devices for sound generation and vibrotactile stimulation,[32,50] the DEA audio-tactile button requires a single active DE element to produce both outputs, in addition to generating the tactile and the acoustic stimuli in a perfectly co-located manner. In the future, this might represent an interesting paradigm for the development of advanced rendering interfaces capable of optimally combining acoustic and tactile stimulation.[51,52]

3. Conclusion

We presented a principle to develop multi-function dielectric elastomer actuators (DEAs) able to concurrently produce linear actuation and sound. We achieved such multi-functionality by taking advantage of the complex dynamic response of a cone DEA layout. This consists in annular dielectric elastomer (DE) membrane deformed out-of-plane by an elastic element, holding at its center a heavy structural element, called output disc (OD), which is free to move in the axial direction. Although the cone DEA layout has been used in the past as linear actuator or loudspeaker, the different dynamics that lie behind these different operating modes had been barely understood to date. We observed that, because of the large difference in mass between OD and DE membrane, the frequency response of the system shows an isolated pumping mode (corresponding to a linear motion of the OD) and a series of structural modes (corresponding to transversal vibrations of the membrane), whose pass-band presents little or no overlap with that of the pumping mode. Providing the DEA with a high-frequency voltage input (with a frequency in the range of the mid/upper-mid audible range) only excites the structural modes and allows generating sound, while leading to a negligible motion of the OD. Exciting the DEA with a lower-frequency input, in contrast, produces a linear stroke of the OD, with negligible sound generation (in contrast to what happens in conventional coil-based loudspeakers with rigid acoustic diaphragm). In this work, we proved that exciting the DEA with a multi-chromatic signal, given by the sum of two independent terms, a high-amplitude lower-frequency (LF) term and a low-amplitude higher-frequency (HF) term, allows achieving linear actuation (which is unaffected by the HF excitation) while at the same time generating sound (which is only a result of the structural modes' excitation).

We built a PDMS-based cone-DEA with diameter of 30 mm, featuring a multi-layer layout consisting of three 50 μm DE membranes, biased off plane by a negative-stiffness buckled-beam spring. The DEA produces linear strokes on the order of 1 mm subject to a static electric field on the order of 90 kV mm^{-1}.

In the range 800–5000 Hz, the DEA generates sound with levels over 60 dB (with peaks over 80 dB over specific frequency ranges), subject to HF electric field variations on the order of 4 kV mm^{-1}. We characterized the response of the DEA in the presence of multi-frequency (LF+HF) inputs both in free conditions (with the OD free to move under no load) and in blocking conditions. The LF component causes a beat in the sound response (with level variations of up to 10 dB over time), due to the DEA nonlinear response. Such effect can be mitigated via an LF compensation of the HF signal amplitude (i.e., increasing the HF excitation amplitude when the superposed LF input is minimum, and viceversa). Although the compensation strategy used in this work is based on a simple heuristics, the results suggest that there exists margin for further reducing or eliminating the beat distortion, for example, by resorting to model-based control policies, built upon nonlinear models of the system.

We presented simple proof-of-concept examples that provide a practical demonstration of the DEA's ability to produce multiple outputs (linear actuation and sound) in practical scenarios. We jointly used the DEA as speaker and metronome, playing music (with average level of 62 dB) while at the same time beating the tempo of the tune through a linear motion of the OD (0.8 mm stroke). We then proved that the DEA can play music when a load of at least 20 g (i.e., a force more than five times larger than the electrostatic axial force variation induced by the HF actuation signal) is applied on the OD, and lift up the load (via a superposed electric field variation on the order of 70 kV mm^{-1}) while still playing the tune. Finally, we used the DEA as a touch detector, a speaker, and a vibrotactile interface at the same time: we used currents measurements to detect deformations impressed by a user through the OD, and trigger an audio-tactile response. The DEA is able to generate sound (60–70 dB) while the user's finger is constraining the OD displacement, while at the same time providing a LF (3–10 Hz) vibrotactile stimulation. These simple examples suggest that the proposed multi-mode principle might provide fresh ground for different applications, for example: wearable tools for musicians, capable to play musical backtracks while providing tactile stimulation; co-located audio-tactile interfaces; and actuators able to provide acoustic feedbacks on their own state (e.g., blocking, overload).

It is finally worth remarking that, although this work focuses on a specific DEA layout (the cone DEA), the same multi-function multi-frequency principle might be applied to other layouts, provided that they combine a lightweight DE membrane and a heavier suspended output mass.

Future developments for the work presented in this paper might include: the investigation of advanced control policies aimed at reducing distortions in the DEA acoustic output in the presence of multi-mode excitation; and the combination of multi-mode actuation and capacitive self-sensing, so as to provide adaptive linear and acoustic responses, based on the impressed levels of deformation.

4. Experimental Section

DEA Materials and Manufacturing: The DE material used for the prototype was PDMS Elastosil 2030 film by Wacker, with initial thickness of 50 μm. The DE membranes were equibiaxially pre-tensioned by a pre-stretch factor of 1.2. Since the DE material is nearly incompressible, the DE layers thickness in the flat pre-stretched configuration was ≈35 μm. Compliant electrodes were made of PDMS (SilGel 612 by Wacker) loaded with carbon-black particles (Orion Printex XE2) and they were screen-printed on the pre-stretched dielectric layers via the procedure described in ref. [53]. The thickness of the printed electrodes was on the order of 10–20% the dielectric layers thickness. The active DEA membrane consisted of a multi-layer dielectric-electrode stack, with three dielectric layers and four electrodes (two high-voltage electrodes and two ground electrodes). Connections between electrodes and metal wires were made with thin copper foils.

The frames holding the pre-stretched DE membrane and the OD were 3D-printed with a photopolymer (clear resin by Formlabs). The DEA assembly (active membrane + holding frames) was mounted onto a 3D-printed ABS case (see Figure 1), holding the NBS and the wires' connectors.

The NBS consisted of two overlapped foils of harmonic steel, with thickness of 50 μm, and with a double-strip cross shape (see Figure S2, Supporting Information). The rigid OD had a mass of 3.9 g, the mass of the NBS was 0.1 g, whereas the membrane mass (electrodes + dielectric) was on the order of 0.1 g.

The out-of-plane deformation of the DEA (measured with a laser sensor ILD1320-25 by Micro-Epsilon) was $h_0 = 5$ mm in the equilibrium position at $v = 0$.

In the tests, the DEA was connected in parallel to and driven by a high-voltage amplifier Trek 609E-6. The input voltage waveforms for the amplifier were generated using the analog output channels of the electronic boards used for control and data acquisition (as described in the following paragraphs). The high-voltage amplifier had maximum output voltage of 4 kV, DC gain of 1000 (with accuracy of at least 0.1 %), nominal output noise below 80 mV, and small-signal bandwidth (−3 dB) greater than 35 kHz.

A same DE sample was used for all the experiments presented in this paper, which were carried out over a time span of ≈40–60 days after the sample fabrication, for a total estimated active working time on the order of 10 h.

Vibro-Acoustic and Multi-Frequency Tests: Measurements of velocity (Figure 2a) and OD stroke (Figures 3 and 4) had been carried out using 3D doppler laser vibrometer PSV-500 3D by Polytec.[26] The average velocity spectrum in Figure 2a had been obtained by measuring a grid of 68 points over the DEA surface (64 on the electrode surface and four on the OD), and calculating the average of the spectra of the axial velocity components (perpendicular to the OD) over all points. For the blocking tests in Figures 2b, 3c, and 4, the DEA's OD was rigidly connected to load cell KD34s-5N by MESysteme (with conditioning unit GSV-1A4), through which force measurements were acquired (Figures 3c and 4a). The connection between the load cell and the DEA allowed for regulations of the OD off-plane bias displacement via a screw. Measurements in Figure 4c show absolute force values, and hence include the contribution of the elastic preload of the membrane.

Sound measurements (Figures 2–4) were performed using microphone MM210 by Microtech Gefell (with conditioning module M33), aligned with the DEA axis and located at a distance of 0.35 m from the sample.

For the tests in Figure 2a, the DEA was excited with a chirp signal, $\tilde{v}(t)$, with constant-magnitude frequency-response (as defined in ref. [54]), with time-domain amplitude $V_a = 100$ V, bias $V_b = 2$ kV, and frequency between 0 and 5000 Hz. For the tests of Figure 2b, $\tilde{v}(t)$ was equal to a sweep signal with amplitude $V_a = 100$ V, and frequency linearly varying between 0 and 5000 Hz within a time span of 10 s.

During the tests, the DEA sample and the microphone were held inside a custom-built sound-absorbing chamber with dimensions of 110 × 100 × 80 cm, with walls covered by sound-absorbing foam to minimize sound reverberation from the surroundings (see Supporting Information). The acoustic chamber presents a 48 × 51 cm frontal aperture that allowed optical measurements via the vibrometer (located outside of the chamber). The datasets in Figures 2–4 were acquired using

the analog input channels of the vibrometer. Outputs were generated with the vibrometer's arbitrary waveform generator, at a sample rate of 50 kHz.

Proof-Of-Concept Tests: For the tests in Figures 5 and 6, the same power supply and acoustic equipment (sound absorbing box, microphone at 0.35 m from the DEA) as in the previous tests were used.

For the test in Figure 5, signal generation and data acquisition (48 kHz) were performed with a digital oscilloscope Analog Discovery 2 by Digilent. OD displacements were measured via laser sensor ILD1320-25 by Micro-Epsilon. The acoustic driving signal in both tests (time-beating speaker and sound generation under load) was obtained by normalizing the target sound tracks (from .wav files) and using the resulting signal (with values comprised between −1 and +1) as $\tilde{v}(t)$ in Equation (3). For the test in Figure 5a, the LF component is a square wave with duty cycle of 25% and frequency equal to the tune's tempo (134 BPM). The clicking sound at the beginning/end of the song was a 2000 Hz pulse with exponentially decaying amplitude (time constant: 25 ms). For the test in Figure 5a, the input signal had $V_{min} = 0.8$ kV, $V_{max} = 2.4$ kV, $V_a = 0.2$ kV, and $\alpha = 2.5$ (see Equation (4)). In the test in Figure 5b–d, the input signal had $V_{min} = 0.8$ kV, $V_{max} = 2.6$ kV, $V_a = 0.06$ kV and $\alpha = 4$. The audio tracks used for the tests in Figure 5 were: the *Pokémon Center* jingle (transcribed by Project Nayuki[55]) for the time-beating loudspeaker test (Video S1, Supporting Information and Figure 5a), and an extract from the aria *Der Hölle Rache*, from Mozart's *Die Zauberflöte*, sung by Luciana Serra for the sound generation under load test (Video S2, Supporting Information and Figure 5b–d).

For the tests on the audio-tactile button (Figure 6), real-time control (i.e., touch detection via current measurements; audio-tactile analog outputs) was implemented on an STM32 H743ZI2 microcontroller, whereas data acquisition was carried out with digital oscilloscope Analog Discovery 2. The time-series of the current in Figure 6 were acquired with the power amplifier's current monitor, whereas current measurements used to trigger the audio-tactile response (inset in Figure 6) were collected using a custom built current sensor (same as in ref. [24]) with range of ±200 μA, mounted in series to the DEA (see Figure S8, Supporting Information). A threshold value $i_{th} = 5$ μA was used as a triggering condition for the audio-tactile feedback. An initial bias voltage of 1.6 kV was applied on the DEA. The excitation signal applied upon touch consisted in a HF sinusoidal signal (2000 Hz in the test in Figure 6b) with exponentially decreasing amplitude ($V_a = 0.2$ kV, time constant: 25 ms), followed by a superposed LF square waveform ($V_{min} = 0.8$ kV, $V_{max} = 2.4$ kV, duty cycle 50%, $f_L = 4$ Hz in Figure 6b) and HF sinusoidal pulsated waveform ($V_a = 100$ kV, $f_H = 1500$ Hz) with exponentially decreasing amplitude (time constant: 200 ms). Different values of the excitation frequencies were also tested (see Video S3, Supporting Information). To ensure safety during the test, the exposed DEA electrode was connected to ground (whereas high-voltage was applied on the internal electrodes), the user wore a protecting glove with an internal insulating PTFE coating, and a passive silicone DE pad was applied on the OD (on the surface touched by the user). It is worth remarking that the value of the DEA capacitance (≈1.9 nF) and the involved currents were well below the safety limits (20 mA continuous DC current and >100 nF) identified for DEA applications.[56]

Data Processing: The velocity and sound pressure spectra in Figure 2a were obtained using Polytec's proprietary post-processing software PSV9.1 for vibrometer PSV-500. Among other, the software was used to visualize and identify the mode shapes associated to the different peaks in the spectra.[26]

The OD stroke was obtained by numerical integration of the vibrometer's velocity measurement in Figures 3 and 4 and measured with a laser position sensor in Figure 5. The instantaneous DEA stroke z in Figures 3 and 5 was defined test-wise, setting $z = 0$ in correspondence of the lowest position reached by the DEA in each specific experiment. The stroke in Figure 4a was defined accordingly as the maximum value reached by z (averaged over all peaks) in each considered test.

The measured acoustic signals were post-processed via the Matlab software in order to eliminate low-frequency disturbances (due to surrounding environment and vibrations). This was done by calculating the fast-Fourier transform of the measured acoustic pressure time-series (with Matlab in-built commands), removing low frequency components (below 50 Hz, i.e., approximately 1/3 the natural frequency of the DEA pumping mode) and using the remaining components to reconstruct a filtered version of the signal. The SPL (Figures 2–4) was calculated from the acoustic pressure time-series as

$$SPL = 20\log_{10}(\tilde{p}/p_0) \qquad (5)$$

where $p_0 = 20$ μPa is the reference human hearing threshold, and $\tilde{p}$ is the moving root-mean-square value of the acoustic pressure calculated over a time window with span of 5 ms. This allowed establishing a one-to-one relationship between the instantaneous value of SPL and the instantaneous excitation frequency in Figure 2b, and to obtain time-trends for the SPL in Figures 3 and 4. The variation ranges for the SPL (colored areas) in Figure 4a were calculated from the maxima and minima (average over the different fluctuations) of the SPL time-series.

Supporting Information

Supporting Information is available from the Wiley Online Library or from the author.

Conflict of Interest

The authors declare no conflict of interest.

Data Availability Statement

The data that support the findings of this study are available from the corresponding author upon reasonable request.

[1] R. Pelrine, R. Kornbluh, Q. Pei, J. Joseph, *Science* **2000**, *287*, 836.

[2] J. Shintake, V. Cacucciolo, H. Shea, D. Floreano, *Soft Rob.* **2018**, *5*, 466.

[3] H. Zhao, A. M. Hussain, A. Israr, D. M. Vogt, M. Duduta, D. R. Clarke, R. J. Wood, *Soft Rob.* **2020**, *7*, 451.

[4] E. Hajiesmaili, D. R. Clarke, *J. Appl. Phys.* **2021**, *129*, 151102.

**ADVANCED
SCIENCE NEWS**

www.advancedsciencenews.com

**ADVANCED
FUNCTIONAL
MATERIALS**

www.afm-journal.de

[5] Y. Chen, L. Agostini, G. Moretti, M. Fontana, R. Vertechy, *Smart Mater. Struct.* **2019**, *28*, 114001.

[6] C. Keplinger, T. Li, R. Baumgartner, Z. Suo, S. Bauer, *Soft Matter* **2012**, *8*, 285.

[7] H. Zhao, A. M. Hussain, M. Duduta, D. M. Vogt, R. J. Wood, D. R. Clarke, *Adv. Funct. Mater.* **2018**, *28*, 1804328.

[8] J. Shintake, S. Rosset, B. Schubert, D. Floreano, H. Shea, *Advanced Mater.* **2016**, *28*, 231.

[9] G. Berselli, R. Vertechy, G. Vassura, V. Parenti-Castelli, *IEEE/ASME Trans. Mechatron.* **2011**, *16*, 67.

[10] M. Hodgins, A. York, S. Seelecke, *Smart Mater. Struct.* **2013**, *22*, 094016.

[11] G.-K. Lau, H.-T. Lim, J.-Y. Teo, Y.-W. Chin, *Smart Mater. Struct.* **2014**, *23*, 025021.

[12] C. Cao, X. Gao, A. T. Conn, *Adv. Mater. Technol.* **2019**, *4*, 1900128.

[13] P. Linnebach, G. Rizzello, S. Seelecke, *Smart Mater. Struct.* **2020**, *29*, 075021.

[14] O. A. Araromi, I. Gavrilovich, J. Shintake, S. Rosset, M. Richard, V. Gass, H. R. Shea, *IEEE/ASME Trans. Mechatron.* **2014**, *20*, 438.

[15] S. Shian, K. Bertoldi, D. R. Clarke, *Adv. Mater.* **2015**, *27*, 6814.

[16] M. Duduta, D. R. Clarke, R. J. Wood, in *2017 IEEE Int. Conf. on Robotics and Automation (ICRA)*, IEEE, Piscataway, NJ **2017**, pp. 4346–4351.

[17] X. Ji, X. Liu, V. Cacucciolo, Y. Civet, A. El Haitami, S. Cantin, Y. Perriard, H. Shea, *Adv. Funct. Mater.* **2021**, *31*, 2006639.

[18] R. Heydt, R. Pelrine, J. Joseph, J. Eckerle, R. Kornbluh, *J. Acoust. Soc. Am.* **2000**, *107*, 833.

[19] T. Sugimoto, A. Ando, K. Ono, Y. Morita, K. Hosoda, D. Ishii, K. Nakamura, *J. Acoust. Soc. Am.* **2013**, *134*, 5EL432.

[20] E. Garnell, O. Doaré, C. Rouby, *J. Acoust. Soc. Am.* **2020**, *147*, 1812.

[21] K. Jung, K. J. Kim, H. R. Choi, *Sens. Actuators, A* **2008**, *143*, 343.

[22] T. A. Gisby, B. M. O'Brien, I. A. Anderson, *Appl. Phys. Lett.* **2013**, *102*, 193703.

[23] G. Rizzello, D. Naso, A. York, S. Seelecke, *Smart Mater. Struct.* **2016**, *25*, 035034.

[24] G. Rizzello, P. Serafino, D. Naso, S. Seelecke, *IEEE Trans. Rob.* **2019**, *36*, 174.

[25] J. Fox, N. Goulbourne, *J. Mech. Phys. Solids* **2009**, *57*, 1417.

[26] G. Moretti, G. Rizzello, M. Fontana, S. Seelecke, *Mech. Syst. Signal Process.* **2022**, *168*, 108677.

[27] G. Moretti, G. Rizzello, M. Fontana, S. Seelecke, in *Electroactive Polymer Actuators and Devices (EAPAD) XXIII*, Vol. *11587*, SPIE, Bellingham, WA **2021**, p. 115871K.

[28] G. Moretti, G. Rizzello, M. Fontana, S. Seelecke, in *Electroactive Polymer Actuators and Devices (EAPAD) XXIV*, Vol. *12042*, SPIE, Bellingham, WA **2022**, pp. 102–112.

[29] G. Frediani, D. Mazzei, D. E. De Rossi, F. Carpi, *Front. Bioeng. Biotechnol.* **2014**, *2*, 31.

[30] H. Phung, P. T. Hoang, H. Jung, T. D. Nguyen, C. T. Nguyen, H. R. Choi, *IEEE/ASME Trans. Mechatron.* **2020**, *26*, 2495.

[31] Q. Van Duong, V. P. Nguyen, A. T. Luu, S. T. Choi, *Sci. Rep.* **2019**, *9*, 13290.

[32] M. E. Altinsoy, S. Merchel, in *Int. Conf. on Haptic and Audio Interaction Design*, Springer, Berlin **2009**, pp. 136–144.

[33] A. Faeth, C. Harding, *ACM Trans. Comput.-Hum. Interact. (TOCHI)* **2014**, *21*, 3.

[34] T. Mirfakhrai, J. D. Madden, R. H. Baughman, *Mater. Today* **2007**, *10*, 30.

[35] N. Hosoya, H. Masuda, S. Maeda, *Appl. Acoust.* **2019**, *148*, 238.

[36] M. Kleiner, *Acoustics and Audio Technology*, J. Ross Publishing, Fort Lauderdale, FL **2011**.

[37] W. Kaal, S. Herold, *IEEE/ASME Trans. Mechatron.* **2010**, *16*, 24.

[38] M. Shrestha, Z. Lu, G.-K. Lau, *ACS Appl. Mater. Interfaces* **2018**, *10*, 39942.

[39] C. Cao, X. Gao, S. Burgess, A. T. Conn, *Extreme Mech. Lett.* **2020**, *35*, 100619.

[40] J. Fox, N. Goulbourne, *J. Mech. Phys. Solids* **2008**, *56*, 2669.

[41] T. Hiruta, N. Hosoya, S. Maeda, I. Kajiwara, *Int. J. Mech. Sci.* **2021**, *191*, 106049.

[42] S. Nalbach, G. Rizzello, S. Seelecke, *J. Vib. Acoust.* **2019**, *141*, 5.

[43] G. Rizzello, M. Hodgins, D. Naso, A. York, S. Seelecke, *Smart Mater. Struct.* **2015**, *24*, 094003.

[44] Z. Suo, *Acta Mech. Solida Sin.* **2010**, *23*, 549.

[45] M. Jabareen, M. Eisenberger, *J. Sound Vib.* **2001**, *240*, 409.

[46] F. Klug, C. Endl, S. Solano-Arana, H. F. Schlaak, in *Electroactive Polymer Actuators and Devices (EAPAD) XXI*, Vol. *10966*, SPIE, Bellingham, WA **2019**, p. 109662I.

[47] E. Garnell, C. Rouby, O. Doaré, *Smart Mater. Struct.* **2021**, *30*, 2.

[48] D. A. Mahns, N. Perkins, V. Sahai, L. Robinson, M. Rowe, *J. Neurophysiol.* **2006**, *95*, 1442.

[49] H. H. King, R. Donlin, B. Hannaford, in *2010 IEEE Haptics Symp.*, IEEE, Piscataway, NJ **2010**, pp. 95–99.

[50] L. Turchet, R. Nordahl, S. Serafin, A. Berrezag, S. Dimitrov, V. Hayward, in *2010 IEEE Int. Workshop on Multimedia Signal Processing*, IEEE, Piscataway, NJ **2010**, pp. 269–273.

[51] M. E. Altinsoy, in *Proc. of the Tenth Int. Congress on Sound and Vibration*, Citeseer, Princeton, NJ **2003**, pp. 3831–3838.

[52] M. E. Altinsoy, *Acoust. Sci. Technol.* **2020**, *41*, 173.

[53] B. Fasolt, M. Hodgins, G. Rizzello, S. Seelecke, *Sens. Actuators, A* **2017**, *265*, 10.

[54] Polytec GmbH, *Polytec Scanning Vibrometer - Theory Manual*, Waldbronn, Germany **2010**.

[55] Project Nayuki web site, https://www.nayuki.io/page/transcription-of-pokemon-game-boy-music, (accessed: June 2022).

[56] S. Pourazadi, A. Shagerdmootaab, H. Chan, M. Moallem, C. Menon, *Smart Mater. Struct.* **2017**, *26*, 115007.

2201889 (12 of 12)